

Channel Modeling of IoT Phantom Networks: Communications in the THz Band

Sudip Misra · Anandarup Mukherjee ·
Pallav Kumar Deb

Received: date / Accepted: date

Abstract The new paradigm of Phantom Networks proposes the deployment of aurally suspended nano-nodes communicating with one another in the THz band for bridging disjoint Internet of Things (IoT) communication infrastructures. We characterize and evaluate the feasibility of single-hop THz band communication between these aurally suspended nano-nodes. Considering an omnidirectional receiver consisting of a planar array of antennas in the conceptualized nano-nodes, we perform an analysis of the signals from different angles in the THz band. To account for the changing environmental conditions in the atmosphere, we consider spreading and molecular absorption as the affecting factors in communication. Further, as additive white Gaussian noise does not affect high-frequency signals, we model the inter-node communication effect on temperature and bandwidth-dependent Johnson-Nyquist noise. Through extensive simulations, we perform a study of the behavior of channel capacities and bit error rates. Our analysis also shows that while transmitting over minimal distances, the effect of spreading increases by 18% for increasing frequencies from 1 to 10 THz. Further, on limiting the angle of signals within 0 and 180 degrees, we observe almost 25% deterioration of the signal as the frequency range increases.

Keywords Nano-networks · THz communication · Channel modelling · Phantom Networks · Spreading · Johnson-Nyquist noise · Aerial nano-nodes

S. Misra
Indian Institute of Technology Kharagpur, India
E-mail: sudipm@iitkgp.ac.in

A. Mukherjee
Cambridge University, United Kingdom
E-mail: anandarupmukherjee@ieee.org

P. K. Deb
Indian Institute of Technology Kharagpur, India
E-mail: pallv.deb@iitkgp.ac.in

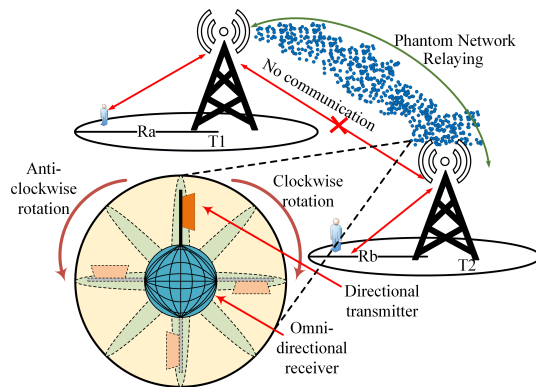


Fig. 1: Nano-node for *Phantom Networks* with directional transmitter and an omni-directional receiver.

1 Introduction

The recently envisioned paradigm of *Phantom Networks* (Misra and Mukherjee, 2020) proposes an intangible network of densely deployed aerial nano-nodes, which helps in bridging disjoint communication infrastructures in the Internet of Things (IoT) environments. It proposes a *deployment system* responsible for releasing an aqueous mist of nano-nodes in the air and a network of *nano-nodes* for communication relaying in the THz band. Fig. 1 outlines the overview of this paradigm, which is envisioned to be useful in IoT applications such as those for disaster-hit areas, military communications, Internet of Vehicles (IoV), and others. In this work, we characterize the one-hop communication of the nano-nodes in this paradigm. As the rest of the communication follows a daisy-chain pattern, analogous to this one-hop transmission with additional factors such as the direction of movement, wind, signal interference, and others, this study forms the initial backbone for all communications of the *Phantom Networks* paradigm.

The free movement of the aerial nano-nodes in the atmosphere after their deployment increases the challenge of maintaining reliable communication between the nano nodes. Considering the advantages of beamforming in high-frequency communications (Xia and Jornet, 2019), we envision the nano-nodes in *Phantom Networks*, as shown in Fig. 1. The *transmitter* consists of a directional antenna and the *receiver* consists of an omnidirectional planar array of antennas. Such an arrangement of the receiver antennae allows the nano-nodes to be omnidirectional receivers, irrespective of their movement and rotation in 3D space. On the other hand, the transmitter's movement introduces the challenge of transmitting only at favorable azimuth and zenith angles. However, the determination of the transmission angle while the nodes rotate is beyond the scope of this work.

1.1 Motivation

The nano-nodes in the plume, envisioned by the *Phantom Networks*, are proximal to one another, which makes them suitable for THz communication bands due to their limited transmission ranges (Sarieeddeen et al., 2019). Existing literature shows that such high-frequency communication channels are much different from the current GHz band. For instance, the presence of obstacles with smooth surfaces for the GHz band, behave as rough surfaces for communication in the THz band. Although researchers have studied the THz channel, the environment for *Phantom Networks* is much different from the traditional ones. While the effects of diffraction, reflection are negligible in this paradigm, other factors, such as interference, high mobility of nodes, directional communications, and other similar factors, need addressing. Additionally, these nano-nodes are affected by environmental conditions, which mandates the need for unique solutions in each case. To address these issues and ensure data transmission from one point to another, we present this work as a foundation to the communication model of *Phantom Networks*.

1.2 Contributions

Communication among the nano-nodes in *Phantom Networks* is challenging in terms of mobility, environmental changes, and other factors. Such challenges need unique solutions in each scenario, which needs a common backbone communication model. In this work, we design and analyze a one-hop communication model for the nano-nodes in the aerially suspended atmospheric plume of nano nodes. Towards this, the primary contributions in this work are:

- **Backbone communication model:** We design a communication model and analyze the one-hop communication among the nano-nodes in *Phantom Networks*. This is a backbone communication model for all our works in the future.
- **Granular parameters:** In this work, we consider parameters such as the angle of transmission, frequency, and distance, to analyze the THz band's behavior for inter-node communication.
- **Analysis:** We present a detailed analysis considering attenuating factors and its effect on signals, channel capacity, and bit error rate. These factors help understand the nature of communication within the plume of nano-nodes and open scope for all future works.

It may be noted that we focus only on the communication model of the links between the aerial nano-nodes in this work. We refrain from the issues pertaining to possible intermittent aerial networks and routing the packets across them, and we plan to address the same in our extended work. This work is an extension of our work on Phantom Networks (Misra and Mukherjee, 2020), which presents its feasibility and applications in different domains.

2 Related Works

Although the nano-nodes of Phantom networks and communication among them need investigation, the existing literature on nano-node and THz communication helps in envisioning this work. The study of signal power distribution at the transmitters and receivers is a non-trivial entity to quantify precisely. Probability distribution functions (PDFs) help in stochastically analyzing the same. However, different PDFs refer to different conditions. While Rayleigh distribution represents signals from the base stations fixed on the ground, Rician distribution represents the signals from the base stations having 3D movement (drones) (Monemi et al., 2020). However, the severity of fading is much severe in the THz band. To capture such behaviors, Aalo and Zhang (Aalo and Jingjun Zhang, 1999) used Nakagami distribution and analyzed the channel. We envision Nakagami distribution to represent the power distribution and interference among nano-nodes in Phantom networks. However, on the other hand, Hossain *et al.* (Hossain et al., 2019) analyzed the interferences as a combination of amplitudes of received signals instead of power and proposed a PDF for THz communications. Further, in works such as those by Lin *et al.* (Lin et al., 2017) proposed a training model based on time-delay phase shifters for beamforming and also presented hybrid processing for extracting the dominant channel information.

The spreading of signal waves in the THz band is not analogous to those in the lower frequencies. The authors in (Sheikh et al., 2020) studied the scattering of the signals in both smooth and rough surfaces using the Beckmann-Kirchhoff (B-K) model in massive MIMO channels. They proposed maximizing the gains by the multiplexing the scattered signals. In addition to scattering, the signals suffer from multiple other phenomena such as reflection, refraction, diffraction, molecular absorption, and others. Han *et al.* (Han et al., 2015) considered all the mentioned parameters and modelled the THz channel. They presented an in-depth analysis of the channel by exploiting the relation of channel frequency and distance. As directional beams help in increasing the efficiency of such high-frequency signals, the authors in (Xia and Jornet, 2019) proposed a scheme for discovering neighbors. To send directional beams, they also found the neighbors' direction using radiation patterns of the antennas. Researchers have been designing models for THz channels for various applications in healthcare (Rong et al., 2018), Networks-on-Chip (NoC) communications (Chen and Han, 2018), and others. Additionally, Ottaviani *et al.* (Ottaviani et al., 2020) proposed a quantum-based cryptography scheme to deal with the decreasing cell size and maintaining user security and privacy.

Synthesis: Researchers have been designing models for representing THz channels and its interferences from external entities. However, existing literature usually depends on 1) 2D tracing of the nano-node communications or 2) in a bounded region of interest. On the other hand, nano-nodes in Phantom Networks move in unbounded space consisting of 3D movement. Such scenarios make the transmission of data from one end to the other challenging. In this

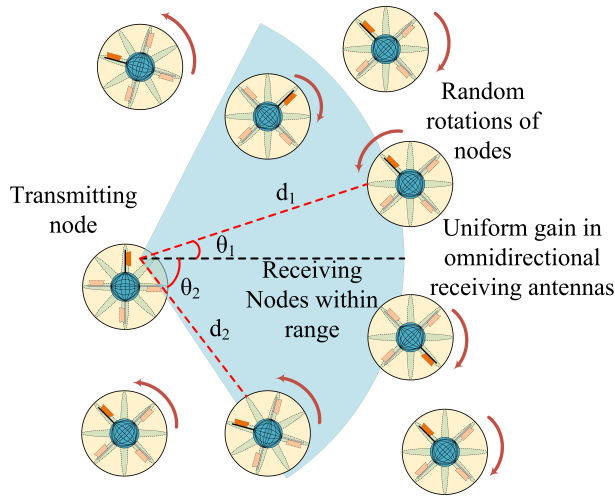


Fig. 2: Directional transmission from one node to another.

work, we provide an analysis of one-hop communication among the nano-nodes to build a skeleton for a daisy chain analysis in the future.

3 Characterizing the Communication Channel

Fig. 2 depicts the nano-nodes after deployment into the atmosphere. As these nodes are suspended in the air, they are arbitrarily susceptible to rotation in the 3D space. Due to the omnidirectional antennas, the rotation does not affect the signal reception across the spherical nano-nodes. However, such rotations affect the directional transmitter, mandating the need for optimal transmission angle and time. Since this work is directed towards the analysis of the channel, we refrain from addressing the rotation of the nano-nodes and plan to solve it in our subsequent works. We characterize the communication channel among the nano-nodes in the atmosphere according to the following sequence:

1. Study the effects of the angle of signal transmission as the nano-nodes in the air are free to rotate and revolve in arbitrary directions. We aim to establish the importance of the transmission angles in the considered environment.
2. Contemplate the effects of molecular absorption (especially due to water vapour) and spreading on the transmitted signal.
3. Since Additive White Gaussian Noise does not effect the signals in the THz band in the same way as in conventional GHz band, we consider and study the effects of the Johnson Nyquist noise.
4. Finally, we study quality of the received signals at the neighboring nano-nodes. It may be noted that the angle of reception does not matter as we recommend using omnidirectional receiver antennas.

We model the Terahertz band (f) considering θ is the angle of the signal, and d is the distance between two nodes under evaluation. For a receiving antenna consisting of a planar array of dimension $\mathcal{N} \times \mathcal{N}$, the normalized power gain is (Balanis, 2005):

$$\mathcal{G}(\theta) = \left(\frac{1}{\mathcal{N}} \frac{\sin^2(\frac{\mathcal{N}}{2}\pi\sin\theta)}{\sin^2(\frac{1}{2}\pi\sin\theta)} \right)^2 \quad (1)$$

Fig. 3 depicts the signal gain at the receiver based on the angle of reception. Ideally, the nano-nodes receive the signals according to Fig. 3a. However, only the cross section receives the signals across 180° as shown in Fig. 3b. Consequently, we limit this work to the range $\theta = [0^\circ, 180^\circ]$. For a signal $x(t)$ from

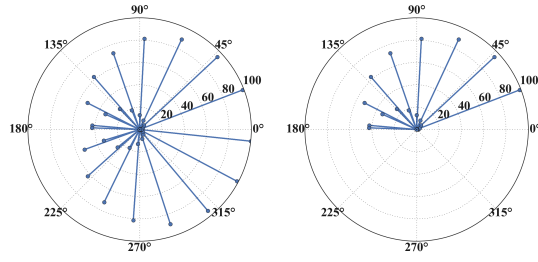
Table 1: List of symbols and their corresponding parameter.

Notation	Parameter
f	THz frequency band
d	Distance
θ	Angle of signal
t	Time
$x(t)$	Signal
c	Speed of light
\mathcal{N}	Dimension of planar array of antennas
h	Fading coefficient
n	Noise
$\mathcal{G}(\theta)$	Normalized signal gain
$S(f)$	Power Spectral Density of signal
$N(T, B)$	Johnson-Nyquist noise due to temperature (T) and bandwidth (B)
$R(f, d)$	Received signal power
A_{spr}	Affect due to spreading
A_{abs}	Affect due to absorption
$k(f)$	Molecular absorption coefficient
P_φ	Probability distribution of φ
SNR	Signal to noise ratio
BER	Bit error rate
\mathcal{C}	Channel Capacity

a transmitter, the receiver receives a signal $y(t)$ in the form $y(t) = h.x(t) + n$, where h is the fading coefficient and n is the noise in the channel. Since the behaviour of the channel changes significantly in the THz band, we focus on the frequency domain rather than the time domain aspects of this channel. For f sub-bands, the attenuation in the signals varies uniquely (Jornet and Akyildiz, 2011). Additionally, the signal power also depends on d as:

$$R(f, d) = \mathcal{G}(\theta)S(f).A(f, d)^{-1} + N(T, B) \quad (2)$$

where $S(f)$ is the power spectral density (PSD) of the transmitted signal, $A(f, d)$ represents the environmental effects, and $N(T, B)$ is the noise due to temperature (T) and bandwidth (B).



(a) Omnidirectional (360°). (b) Directional (upto 180°).

Fig. 3: Gain for omnidirectional and directional receivers with 10×10 planar array of antennas.

The PSD of the signal over time (t) for signal $x(t)$ can be represented as:

$$\begin{aligned} S(f) &= \int_t e^{-2\pi i f t} x(t) dt = \frac{e^{-2\pi i f t}}{-2\pi i f} \int_t x(t) dt \\ &= \tau \frac{e^{-2\pi i f t}}{-2\pi i f}, \text{ where } \tau = \int_t x(t) dt \end{aligned} \quad (3)$$

Signals from the transmitter suffer due to multiple factors such as spreading, reflection, refraction, diffraction, absorption, and other environmental factors. However, the nano-nodes in *Phantom Networks* are in close proximity, which reduces the possibility of reflection, refraction, and diffraction. Due to the nature of deployment of the nodes, we focus on the effects of spreading in free space (A_{spr}) and absorption (A_{abs}) as shown in Fig. 4 and denoted mathematically as $A(f, d) = A_{spr}(f, d) + A_{abs}(f, d)$. The same is represented in decibels (dB) as (Jornet and Akyildiz, 2011):

$$A(f, d)[dB] = 20 \log\left(\frac{4\pi f d}{c}\right) + k(f) d \cdot 10 \log_{10} e \quad (4)$$

In Equation 4, c is the speed of light in free space and $k(f)$ is a molecular absorption constant. It may be noted that in the THz band, the major diminishing factor of the signals from the transmitter is due to absorption by water vapour (Jornet and Akyildiz, 2011).

In contrast, the constructive and destructive noise parameters in the GHz and MHz band do not behave the same manner as in the THz band. For such high frequencies in the THz band, the molecular vibrations triggered due to surrounding temperature has a major impact on the quality of the signal. Considering this factor, we use *Johnson-Nyquist* (Tomasi, 1994) noise in this work. The noise power density is a function of the atmospheric temperature (T) and Bandwidth (B). Mathematically, this noise can be denoted as,

$$N(T, B) = k_B \times T \times B \quad (5)$$

where k_B is the Boltzmann constant.

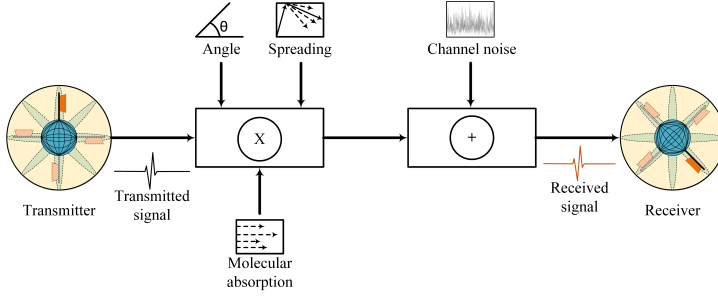


Fig. 4: Overview of channel model.

In this work, we aim to study the variations in the signal arising due to the changes in θ , f , and d , respectively. We jointly calculate the effect on the transmitted signal due to these parameters at the receiver as:

$$P_S(\theta, f, d) = \int_{\theta} \int_f \int_d \mathcal{G}(\theta) S(f) A(f, d)^{-1} \partial\theta \partial f \partial d \quad (6)$$

Since, $S(f)$ and $A(f, d)$ have no dependence on θ , we solve $\int_{\theta} \mathcal{G}(\theta) \partial\theta$ separately as:

$$\begin{aligned} \int_{\theta} \mathcal{G}(\theta) &= \int_{\theta} \left(\frac{1}{(N)} \frac{\sin^2\left(\frac{N}{2}\pi\sin\theta\right)}{\sin^2\left(\frac{1}{2}\pi\sin\theta\right)} \right)^2 \partial\theta \\ \text{Let } x &= \frac{1}{2}\pi\sin\theta \Rightarrow \partial\theta = \frac{2}{\sqrt{1-4x^2}} \partial x \\ &= \int_{\theta} \frac{1}{(N)} \frac{\sin^4(N)x}{\sin^4 x} \frac{2}{\sqrt{1-4x^2}} \partial x \\ &= \frac{2}{(N)} e^{4(N)} \frac{1}{2} \sin^{-1}(\pi\sin\theta) + C \Big|_{\theta} \end{aligned} \quad (7)$$

It may be noted that we use the form $\sin(\theta) = \frac{e^{i\theta} - e^{-i\theta}}{2i}$ while obtaining Equation 7. Integrating the rest of Equation 6 with respect to frequency and distance, we obtain,

$$\begin{aligned}
I_{f,d} &= \int_d \int_f S(f)A(f,d)^{-1} \partial f \partial d \\
&= \int_d \int_f \tau \frac{e^{-2\pi i f t}}{-2\pi i f} \frac{1}{20\log(\frac{4\pi f d}{c}) + k(f)d \cdot 10\log_{10}e} \partial f \partial d \quad (8)
\end{aligned}$$

$$I_{f,d} = \int_d \frac{-E_1(t)\tau}{\pi i} \frac{1}{20\log(\frac{4\pi f d}{c}) + dk(f)10\log_{10}e} \partial d \Big|_f \quad (9)$$

$$\begin{aligned}
\Rightarrow I_{f,d} &= \frac{-E_1(t)\tau}{\pi i} \frac{1}{20c + dk(f)10\log_{10}e} \times \\
&\quad \frac{20cd}{20\log(\frac{4\pi f d}{c}) + dk(f)10\log_{10}e} + C \Big|_{f|d} \quad (10)
\end{aligned}$$

$$\begin{aligned}
P_S(\theta, f, d) &= \frac{2}{N^2} e^{4N} \frac{1}{2} \sin^{-1}(\pi \sin \theta) \frac{-E_1(t)\tau}{\pi i} \times \frac{1}{20c + dk(f)10\log_{10}e} \times \\
&\quad \frac{20cd}{(20\log(\frac{4\pi f d}{c}) + dk(f)10\log_{10}e)} + C \Big|_{\theta|f|d} \quad (11)
\end{aligned}$$

Integrating $I_{f,d}$ with respect to f , we obtain the result in Equation 9. The term $E_1(t)$ is the exponential integral $\int \frac{e^{-xt}}{x} dx$, where $x = -2\pi i f$ and $t \rightarrow \infty$. Upon further integrating Equation 9 with respect to d , we obtain the expression in Equation 10. Combining Equations 7 and 10, we obtain the final expression of $P_S(s)$ as shown in Equation 11.

The expression in Equation 11 provides the effect on the signal due the parameters θ , f , and d , respectively. However, in this work, we intend to determine the empowering values of θ and d over f , ranging from 1 – 10 THz. To highlight the effects of f on both θ and d , we find the marginal distributions. The marginal distribution of the distance for the signal ($P_D(d)$) is the integration of Equation $P_S(\theta, f, d)$ with respect to θ and f , respectively. Mathematically,

$$P_D(d) = \int_f \int_\theta P_S(\theta, f, d) \partial \theta \partial f$$

Upon expansion, we obtain Equation 16. For ease of understanding, we extract only the θ terms and evaluate the integral separately:

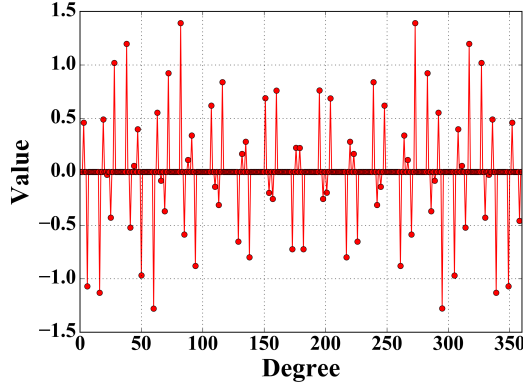


Fig. 5: Suitable degrees of signal for $\sin^{-1}(\pi \sin \theta)$.

$$\begin{aligned}
 I_{\theta}^d &= \int \sin^{-1}(\pi \sin \theta) \partial \theta \\
 \text{Let } x &= \pi \sin \theta \implies \partial \theta = \frac{\partial x}{\pi \cos \theta} \\
 \implies I_{\theta}^d &= \frac{1}{\pi \cos \theta} \int \sin^{-1} x \partial x \\
 &= \frac{1}{\pi \cos \theta} (x \sin^{-1}(x) + \sqrt{1-x^2}) + C \\
 &= \tan \theta \sin^{-1}(\pi \sin \theta) + \frac{\sqrt{1-\pi^2 \sin^2 \theta}}{\pi \cos \theta} + C \quad (12)
 \end{aligned}$$

Due to the presence of π in $\sin^{-1}(\pi \sin(\theta))$ in Equation 12, it is not valid for all values of θ . Fig. 5 depicts the valid θ values for I_{θ} . We consider the zero values are the invalid ones. On integrating the rest of Equation 16 with respect to f , we obtain:

$$I_f^d = \frac{f}{(20 \log(\frac{4\pi f d}{k(f)}) + k(f) d 10 \log_{10} e)} \quad (13)$$

Combining Equations 12 and 13, we obtain the expression for $P_D(d)$ as shown in Equation 17. Similarly, the marginal distribution of the angle of the signal ($P_{\Theta}(\theta)$) is the integration of Equation $P_S(\theta, f, d)$ with respect to f and d , respectively. Mathematically,

$$P_{\Theta}(\theta) = \int_d \int_f P_S(\theta, f, d) \partial f \partial d \quad (14)$$

We obtain Equation 18 upon expansion and Equation 19 on integrating with respect to f . Subsequently, integrating further with respect to d , we obtain

Table 2: Channel evaluation parameters and their ranges.

Variables	Values
Angle (θ)	$0^\circ - 180^\circ$
Frequency (f)	1 – 10 THz
Distance (d)	0 – 10 m
Bandwidth (B)	1 – 6 THz
Boltzmann constant (k_B)	1.38×10^{-23}
Antenna Array (N)	10×10

the expression for the marginal distribution of the angle of the signal ($P_\Theta(\theta)$) as in Equation 20. We determine M_n^d using the *mid point rule*, where

$$M_n^d = \sum_{i=1}^n f(d) \Delta d \quad (15)$$

with $f(d) = \frac{1}{(20 \log(\frac{4\pi f d}{c}) + ad)}$ and $\Delta d = \frac{10^{20} - 1}{n}$ for $d = (0^+, 10^{20})$.

$$P_D(d) = \frac{-e^{4N} E_1(t) \tau 20c}{N^2 \pi i} \int_{\theta} \int_f \sin^{-1}(\pi \sin \theta) \times \frac{d}{(20c + dk(f) 10 \log_{10} e)(20 \log(\frac{4\pi f d}{c}) + dk(f) 10 \log_{10} e)} \partial \theta \partial f \quad (16)$$

$$\Rightarrow P_D(d) = \frac{-e^{4N} E_1(t) \tau 20c}{N^2 \pi i} \left(\tan \theta \sin^{-1}(\pi \sin \theta) + \frac{\sqrt{1 - \pi^2 \sin^2 \theta}}{\pi \cos \theta} \right) \times \frac{d}{(20c + dk(f) 10 \log_{10} e)(20 \log(\frac{4\pi f d}{c}) + dk(f) 10 \log_{10} e)} + C \Big|_{\theta} \Big|_f \quad (17)$$

$$P_\Theta(\theta) = \frac{-e^{4N} E_1(t) \tau 20c \sin^{-1}(\pi \sin \theta)}{N^2 \pi i} \times \int_d \int_f \frac{d}{(20c + dk(f) 10 \log_{10} e)(20 \log(\frac{4\pi f d}{c}) + dk(f) 10 \log_{10} e)} \partial f \partial d \quad (18)$$

$$\Rightarrow P_\Theta(\theta) = \frac{-e^{4N} E_1(t) \tau 20c \sin^{-1}(\pi \sin \theta)}{N^2 \pi i} f \times \int_d \frac{d}{(20c + dk(f) 10 \log_{10} e)(20 \log(\frac{4\pi f d}{c}) + dk(f) 10 \log_{10} e)} \partial d \Big|_f \quad (19)$$

$$\Rightarrow P_\Theta(\theta) = \frac{-e^{4N} E_1(t) \tau 20c \sin^{-1}(\pi \sin \theta)}{N^2 \pi i} f \frac{M_n^d}{k(f) 10 \log_{10} e} + C \Big|_f \Big|_d \quad (20)$$

4 Performance Characterization Metrics

We outline the parameters, which we consider for characterizing the channel among the nano-nodes. In Section 5, we analyze the performance of the THz band channel based on these metrics.

Spreading: This occurs when a signal enters a medium from the transmitter. The change in medium impinges the signal causing its energy to spread in different directions. We calculate the spread in the atmosphere using A_{spr} in Equation 4. Mathematically,

$$A_{spr} = 20 \log \left(\frac{4\pi f d}{c} \right) \quad (21)$$

We evaluate spreading of the signal with increasing distance across different frequencies.

Molecular Absorption: As the electromagnetic (EM) waves pass through a medium, the molecules present in that medium absorb the radiant energy for triggering molecular oscillations. Such absorption of energy affects the signal and we calculate the same using A_{abs} in Equation 4. Mathematically, we represent it as,

$$A_{abs} = k(f) \times d \times 10 \times \log_{10} e \quad (22)$$

Similar to the case of scattering, we evaluate molecular absorption of the signal with increasing distance across different frequencies.

Effects on Signal: We consider granular parameters such as θ , f , and d to characterize the effects on the received signal. Using Equation 11, we jointly represent the effect of each on the signal. We first present the behavior of the signal with varying values of each parameter and then proceed to observe the marginal distributions to get a better insight into the changes induced in the incoming signal.

Marginal Probability Distributions: The marginal distributions of d and θ in Equations 17 and 20 help in presenting an insight on how the parameters affect the signal in different frequencies. The characterization of these distributions helps in determining parameters for transmitting reliable signals over the network.

Channel Capacity: We compute the capacity of the channels among the nano-nodes using the equation:

$$C = BW \times \log_2(1 + SNR) \quad (23)$$

$$\text{where } SNR = \frac{\mathcal{G}(\theta)S(f)A(f, d)^{-1}}{N(T, B)} \quad (24)$$

At constant bandwidth of 1 THz, we present the channel capacities with respect to θ and d .

Bit Error Rate: With respect to varying frequencies, it is important to analyze the error rate in each channel. In this work, we calculate the bit error

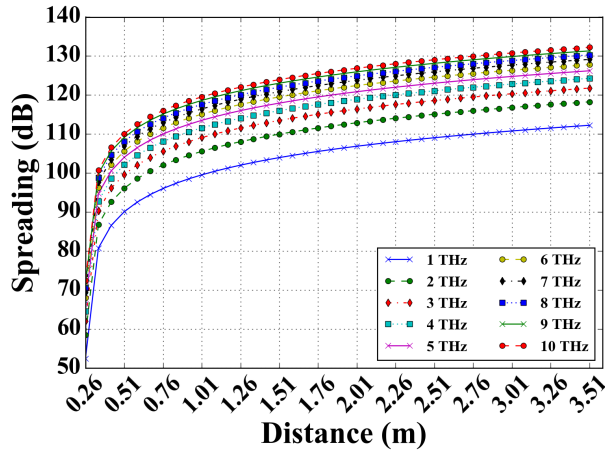


Fig. 6: Spreading (dB) with respect to distance and frequency.

rate (BER) using the equation:

$$BER = 2^{N-1} C_N \times \left(\frac{1}{2SNR} \right)^N \quad (25)$$

We calculate the *signal-to-noise ratio* (SNR) based on the expression in channel capacity. We analyze the BER with varying bandwidths and center frequencies.

5 Evaluation of the THz Band Channel

In this section, we first present our parameters and then perform an analysis of the channel. During the analysis of this work, we use the parameters and their respective ranges, as outlined in Table 2.

5.1 Signal Spreading

One of the prominent effects of atmospheric attenuation is spreading. Fig. 6 depicts the effect of spreading as the frequencies and the distances change. We observe that the effect of spreading follows the same pattern as the distance increases. We attribute the curve in Fig. 6 to the log in equation 21. It may be noted that as the frequency increases from 1 THz to 10 THz, the effect of spreading increases by almost 18.18%.

Physical Significance: As the frequencies increase, the change in the signal spreading is minuscule. Consequently, the communication among the nano-nodes is favourable when the distance is limited to less than 0.25 m. Such

Table 3: Absorption coefficients.

Frequency (THz)	1	2	3	4	5	6	7	8	9	10
$k(f)$ (m^{-1})	0.3	0.1	1.1	0.75	0.3	3	0.1	0.2	2	0.9

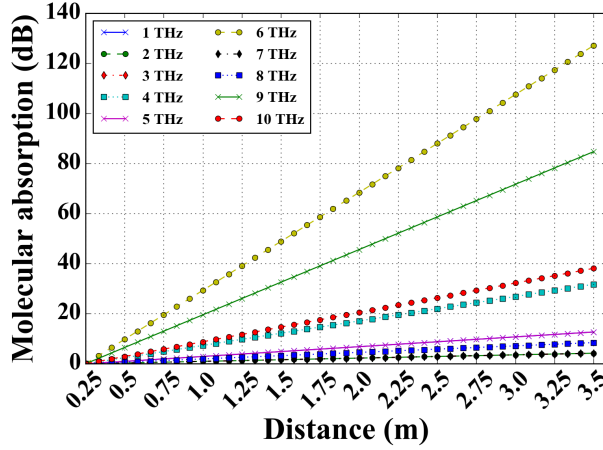


Fig. 7: Molecular absorption (dB) with respect to distance and frequency.

small distances are intuitively suitable for the nano-nodes as they are originally intended to be in close proximity to one another in the atmosphere.

5.2 Molecular Absorption

In an environment, considering the deployment of the proposed aerial network, another realistic and significant signal attenuating factor is water vapor (Jornet and Akyildiz, 2011). It may be noted that the values of $k(f)$ keep resonating continuously across all frequency values. We round the frequencies and list the values of $k(f)$ in Table 3. Fig. 7 depicts the molecular absorption by water vapor with varying distances and frequencies. As expected, we observe that the absorption increases as the distance increases. However, we observe particularly higher absorption rates at 6 and 9 THz compared to the other frequencies. We attribute this behavior to the higher absorption coefficients at these frequencies, which affects the signal quality.

Physical Significance: The results from Fig. 7 highlight the varying behavior of the signal over increasing distances with varying frequencies. Such characteristics opens the scope for selecting frequency channels based on the distance to which the nano-nodes need to transmit their signal.

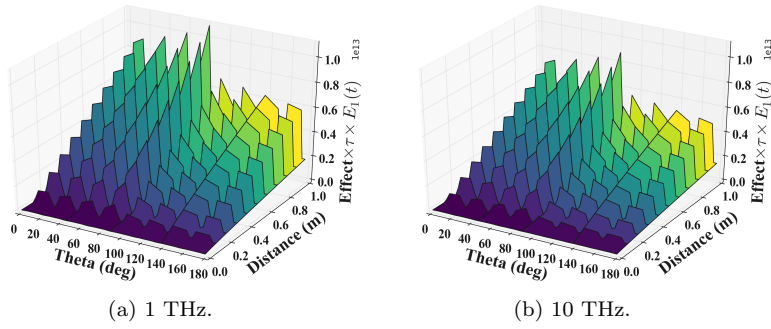


Fig. 8: Effect on signal due to varying frequencies.

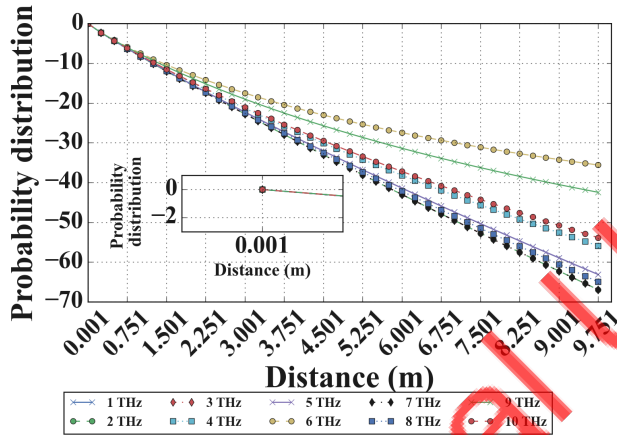


Fig. 9: Probability distribution of distance at varying frequencies.

5.3 Effects on Signal

From the discussions in Sections 5.4 and 5.5, we set $\theta = [0, 180]$ degrees and $d = [0.001, 1]$ m. Fig. 8 depicts the effect on the signals at the receivers based on these values. We observe that at both 1 THz (Fig. 8a) and 10 THz (Fig. 8b), the change in behavior of the signal follows a similar pattern. However, the 1 THz frequency band affects the signal more by almost 23%, compared to the 10 THz frequency band. We attribute this to the scattering, molecular absorption, as well as the signal gains at particular reception angles.

Physical Significance: We observe that as the frequencies increase, the environmental effects on the signal decrease. Due to such observations, we aspire to use higher frequencies for *Phantom Networks*. This entails dense deployment of the nano-nodes as higher frequencies have lower wavelength, which further reduces the transmission distance.

5.4 PDF of Distance

We calculate the $P_D(d)$ values based on Equation 17. With varying frequencies and distances, we observe the probability distribution trend as shown in Fig. 9. As the distances increase, the PDF demonstrates negative values. Probability values of zero usually depicts an impossible event. However, we relax the *Kolmogorov's axioms* in this work.

Physical Significance: These negative values show that such distances are not favourable in *Phantom Networks*. We observe that the PDF demonstrates negative values for longer distances and is close to zero on distances in the range of 0.001 m (Fig. 9). We infer that the communications among the nano-nodes is successful at very small distances. Such distances are suitable for the plume of nano-nodes as it helps in avoiding interferences on the neighboring nodes which are relatively further away.

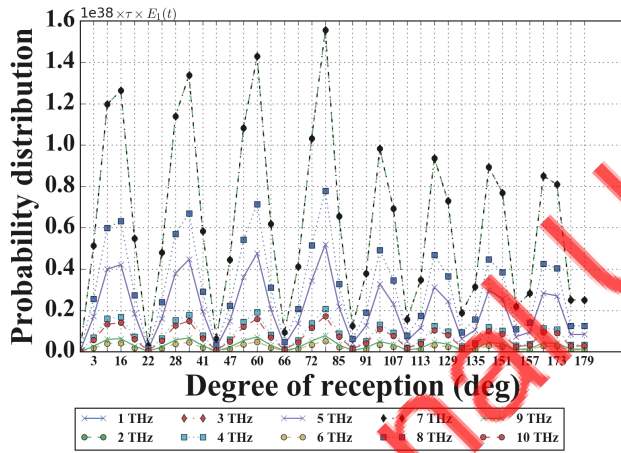


Fig. 10: Probability distribution of theta.

5.5 PDF of Reception Angle

We calculate the $P_\theta(\theta)$ values based on Equation 20. Fig. 10 depicts the PDF of the signal reception angle on the receiver antennas. The oscillating values is due to the presence of sinusoidal harmonics and due to the varying range of θ from 0 to 180 degrees. However, based on the varying frequencies, we observe higher amplitudes in case of 7 and 2 THz. Further, we observe lower amplitudes at 5 and 8 THz. The rest of the frequencies have similar range of PDF for θ . We attribute these to the varying values of $k(f)$ at different frequencies.

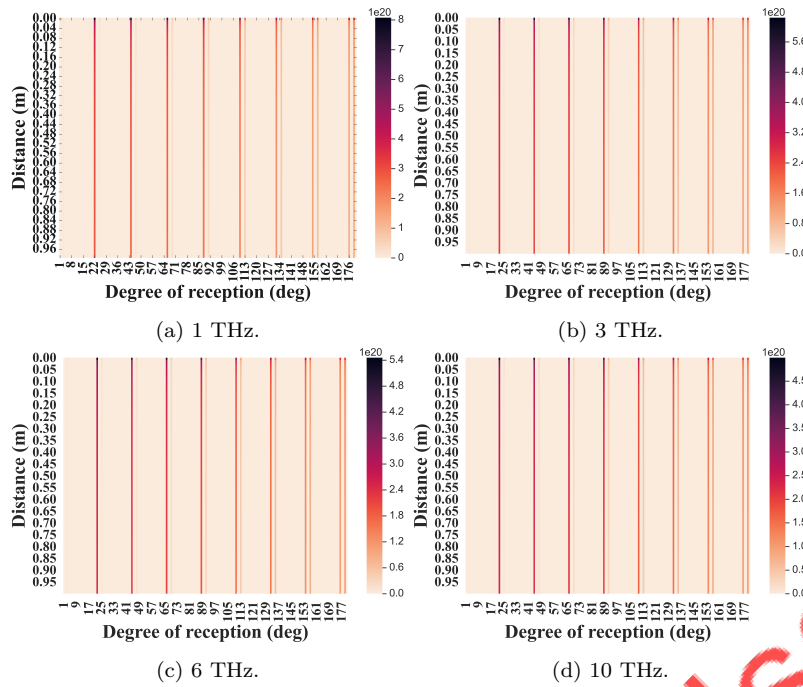


Fig. 11: Channel capacities with varying frequencies over 1 THz bandwidth.

Physical Significance: For establishing efficient communication among the nano-nodes, apart from selection of appropriate frequency channels, the determination of optimal angles of transmission and reception is important. We plan to address this objective in our future work.

5.6 Channel Capacity

We set the signal PSD $S(f)$ to unit power and compute the channel capacity using a fixed B of 1 THz and varying center frequencies (f). As discussed in Equation 12 and Fig. 5, we observe the gain on particular values of θ . Similarly, we observe higher channel capacities for certain θ values in Fig. 11. Additionally, as the distance increases, the capacities decrease across all the angles. However, as the center frequencies increase for a constant B , the channel capacity tends to decrease. For instance, on increasing f from 1 THz in Fig. 11a to 10 THz in Fig. 11d, we observe a reduction in \mathcal{C} by almost 47%.

Physical Significance: For fixed B , the nano-nodes need to choose a lower range of frequency channels to obtain higher channel capacities. In case the lower frequency channels are busy, changes in B before transmitting using higher frequency channels, will prove beneficial for the nano-nodes.

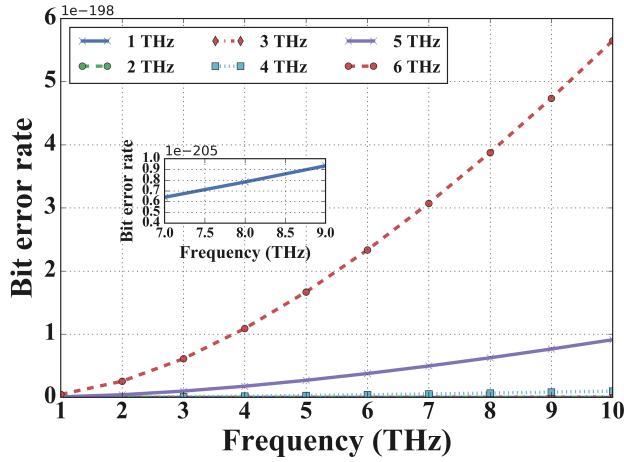


Fig. 12: Bit error rate with varying frequencies and bandwidth.

Table 4: Comparison and suitability of communication technologies for phantom networks.

Category	Data rate	Distance	Suitability for Phantom Networks
4G/LTE Jo and Shim (2019)	10 Mbps	100 Km	Low
WiFi Ahmad et al. (2020)	220 Mbps	50 m	Medium
THz band (proposed work)	6×10^4 Pbps	Less than 1m	High

5.7 Bit Error Rate

Fig. 12 depicts the BER with varying B from 1–6 THz and carrier frequencies f from 1–10 THz using the Equation 25. We observe minuscule BERs in case of the THz band. We attribute this to the absence of the White Gaussian Noise in such high frequencies. However, we observe that as the bandwidth increases, the BER increases exponentially with increasing f . This increase in BER is because as the frequency increases, the data rate also increases (Fig. 11), which causes in an increase in the number of errors. Interestingly, although we observe an exponential increase in BER, for frequencies such as the 4 THz one, the increase is relatively linear.

Physical Significance: For transmitting error free signals from one nanonode to another, we need to determine appropriate carrier channels based on B .

5.8 Suitability of Communication Technologies

In this work, we characterize the communication channels between the nano-nodes in the THz band. There are other communications such as Long Term Evolution (LTE) Jo and Shim (2019) and WiFi Ahmad et al. (2020) that are widely deployed across different applications. Table 4 presents a comparison of these technologies with that of the THz band. We observe that while LTE networks offer a large communication range, the data rate in LTE networks is much lower (10 Mbps) than the other two. On the other hand, data rate in the WiFi networks is relatively higher (220 Mbps) than the LTE networks and much lower than the THz band. The communication range is limited to 50 meters. Such difference in the data rates and the communication distance is due to the varying bandwidths and transmission signal power. It may be noted that as the bandwidth increases, the distance/transmission range decreases. This phenomenon is further evident in the THz band, where we observe data rates in the range of Petabyte per seconds (Fig. 11), the transmission distance reduces to less than 1 meter.

Physical Significance: The THz band offers high data rates in comparison to the conventional technologies. Further, as the nano-nodes in the Phantom Networks are densely concentrated in the atmosphere, communication ranges of less than 1 meters does not hamper the communication links. We account for these conditions and from our observations in Table 4, we infer that the THz band is the most suitable technology for the Phantom networks paradigm.

6 Scope and Limitations

This work focuses primarily on modeling the channel, particularly for characterizing the communication among the nano-nodes of *Phantom Networks*. However, the scope of this model may be extended to any THz communication channels with a deeper insight to the angle of transmitted signal, frequency, and distance from the source. Additionally, this work is limited to a single hop in a multi-hop relay channel, which opens scope for designing multi-hop routines based on this underlying model. As the channel model in this work is performed for the THz band, reliable communication is limited to very small distances. Additionally, mathematical expressions do not confirm successful reception of signal in all the angles of transmission. Summarily, the non-analogous characteristics of the THz band in comparison to GHz and MHz communications mandates the need for simultaneous optimization of θ , f , and d , respectively.

7 Conclusion

In this work, we formulated a channel model for representing communications among the plume of aerielly-suspended nano-nodes, corresponding to the recent paradigm of the *Phantom Networks*. The Phantom Networks helps in overcoming communication voids in IoT infrastructures. Although this work

pursues a one-hop model, the relaying along the communicating aerial nano-nodes will follow the same trend in the form of a daisy chain. In this model, we considered granular parameters such as angle of transmission, frequency, and distance and presented a detailed analysis of their effects on the THz band channel and inter-communications among the aerial nano-nodes.

In the future, we plan to extend our work by providing a model for the end-to-end communication between two access points using the plume of nano-nodes in the context of *Phantom Networks*. Further, we also plan to determine the optimal transmission conditions for the arbitrarily rotating nano-nodes with directional transmitters. Currently, we limited ourselves from considering mobility and directional transmission of the signal from nano-nodes moving freely in 3D space. Towards this, we plan to consider environmental factors like wind, temperature, and others which affect the channel conditions.

References

- Aalo VA, Jingjun Zhang (1999) On the effect of cochannel interference on average error rates in Nakagami-fading channels. *IEEE Communications Letters* 3(5):136–138
- Ahmad R, Soltani MD, Safari M, Srivastava A, Das A (2020) Reinforcement learning based load balancing for hybrid lifi wifi networks. *IEEE Access* 8:132273–132284
- Balanis CA (2005) *Antenna Theory: Analysis and Design*. Wiley-Interscience, USA
- Chen Y, Han C (2018) Channel modeling and analysis for wireless networks-on-chip communications in the millimeter wave and terahertz bands. In: *Proceedings of IEEE Conference on Computer Communications Workshops (INFOCOM WKSHPs)*, pp 651–656
- Han C, Bicen AO, Akyildiz IF (2015) Multi-Ray Channel Modeling and Wide-band Characterization for Wireless Communications in the Terahertz Band. *IEEE Transactions on Wireless Communications* 14(5):2402–2412
- Hossain Z, Mollica CN, Federici JF, Jornet JM (2019) Stochastic Interference Modeling and Experimental Validation for Pulse-Based Terahertz Communication. *IEEE Transactions on Wireless Communications* 18(8):4103–4115
- Jo S, Shim W (2019) Lte-maritime: High-speed maritime wireless communication based on lte technology. *IEEE Access* 7:53172–53181
- Jornet JM, Akyildiz IF (2011) Channel Modeling and Capacity Analysis for Electromagnetic Wireless Nanonetworks in the Terahertz Band. *IEEE Transactions on Wireless Communications* 10(10):3211–3221
- Lin C, Li GY, Wang L (2017) Subarray-based coordinated beamforming training for mmwave and sub-thz communications. *IEEE Journal on Selected Areas in Communications* 35(9):2115–2126
- Misra S, Mukherjee A (2020) ‘Phantom Networks’: The Intangible Shoot-and-Scoot Communication Paradigm for Future Militaries. *IEEE Communications Magazine* 58(2):66–71

- Monemi M, Tabassum H, Zahedi R (2020) On the Performance of Non-Orthogonal Multiple Access (NOMA): Terrestrial vs. Aerial Networks. 2002.00826
- Ottaviani C, Woolley MJ, Erementchouk M, Federici JF, Mazumder P, Pirandola S, Weedbrook C (2020) Terahertz quantum cryptography. *IEEE Journal on Selected Areas in Communications* 38(3):483–495
- Rong Z, Leeson MS, Higgins MD, Lu Y (2018) Nano-rectenna powered body-centric nano-networks in the terahertz band. *Healthcare Technology Letters* 5(4):113–117
- Sarieddeen H, Alouini M, Al-Naffouri TY (2019) Terahertz-band ultra-massive spatial modulation mimo. *IEEE Journal on Selected Areas in Communications* 37(9):2040–2052
- Sheikh F, Gao Y, Kaiser T (2020) A Study of Diffuse Scattering in Massive MIMO Channels at Terahertz Frequencies. *IEEE Transactions on Antennas and Propagation* 68(2):997–1008
- Tomasi W (1994) *Electronic Communication*. Prentice Hall PTR, URL <https://books.google.com.ph/books?id=LXPWxmakFVgC>
- Xia Q, Jornet JM (2019) Expedited Neighbor Discovery in Directional Terahertz Communication Networks Enhanced by Antenna Side-Lobe Information. *IEEE Transactions on Vehicular Technology* 68(8):7804–7814

For Personal Use Only